Hexagonal-Shaped Broadband Compact Scrimp Horn Antenna for Operation in C-Band

Shoaib Anwar Muhammad, Anthony Rolland, Samsul Haimi Dahlan, Ronan Sauleau, *Senior Member, IEEE*, and Hervé Legay

***Abstract*—The performance of compact linearly polarized Short Circular Ring-loaded horn with Minimized cross-Polarization (Scrimp) horns with different aperture sizes is first evaluated using an in-house finite-difference time-domain (FDTD) computer-aided design (CAD) tool. Then, a very short hexagonal Scrimp horn with an aperture size of $1.5\lambda_0$ is designed in C-band; its height is only $1.26\lambda_0$. The experimental results demonstrate that the aperture efficiency is higher than 80% with a reflection coefficient lower than -17 dB over a 12.6% frequency bandwidth. Radiation patterns of excellent quality are measured with a cross-polarization level lower than -28 dB over the entire bandwidth. These antennas are very attractive candidates for high-power focal array configurations in multifeed systems.**

***Index Terms*—Compact feed horns, linear polarization, Scrimp horns, space applications.**

I. Introduction

COMPACT feed elements are widely used for multiband multifeed systems, e.g., [1] and [2], or as single radiating elements in space applications [3]. In particular, C-band global horn antennas are normally used for telemetry, tracking, and control in satellites operating in a geostationary orbit or for providing downlink connectivity from satellite to node. This type of horn is also employed for navigation satellite feeder links in medium Earth orbit. One of the major antenna concerns for those applications is the prohibitive size and mass of such feeds [2]–[4] (especially for small satellites) while keeping a large enough bandwidth.

In this frame, different types of compact feed elements are available in the literature. Here, we focus our attention on purely metallic structures for a possible use in high-power space applications. Compact Potter horns and variants [5], [6] offer excellent performance with a total horn length of a few wavelengths (typically larger than $3\lambda_0$ as reported in [6]). Short backfire antenna elements [7], [8] are more compact (total height $\sim \lambda_0$) and exhibit a satisfactory operational bandwidth (around 8%), but their performance in aperture efficiency [9], [10, Eq. (2)] is limited to aperture sizes smaller than $2\lambda_0$. Recently, compact stacked Fabry–Perot (FP) antennas [10] have been proposed with good performance for a radiating aperture of $1.85\lambda_0$ and a height of around λ_0. They offer an operational bandwidth of more than 10% with good pattern symmetry and aperture efficiency levels.

Another interesting compact horn configuration, known as Short Circular Ring-loaded horn with Minimized cross-Polarization (Scrimp) horn, was introduced in the late 1990s [11], [12]. Experimental results for a multifeed satellite system showed excellent performance for a horn aperture size of $1.7\lambda_0$. The total height of the antenna was around $1.3\lambda_0$. Experimental results provided in C-band demonstrated an aperture efficiency level higher than 77% over a 11.6% frequency band. However, despite their very attractive features, no detailed performance review and application of this concept to other aperture sizes has been reported in literature to the best of the authors' knowledge.

The main objective of this letter is to define the overall performance of such antennas in the perspective of focal array applications with stringent limitations in terms of aperture diameter and antenna height. The main characteristics of optimized Scrimp horn antennas are reported for different antenna aperture sizes in Section II. An in-house finite-difference time-domain (FDTD) technique has been used for the optimization [12]. A compact hexagonal-shaped Scrimp horn is presented in Section III for a better integration into a focal array system with a hexagonal lattice. The experimental results are in excellent agreement with the simulations.

II. Performance Overview of Scrimp Horn Antennas

A. Antenna Geometry

The geometry of the proposed horn antenna is represented in Fig. 1. It consists of a conical horn section fed by a cylindrical waveguide. The coaxial stub section [Fig. 1(b)] is placed at the mouth of the horn with a depth of h_s and it is extended until the antenna aperture (h_c).

The operating principle of the this antenna is based on the excitation and mixing of higher order modes (TM_{11}, TE_{21}) with the fundamental mode (TE_{11}) in order to generate low cross-polarization levels [11], [12].

B. Optimization Tool

To optimize the proposed antenna structure, an in-house optimization tool based on a genetic algorithm coupled with Body of Revolution FDTD (BoR-FDTD) method is employed [12].

Manuscript received February 24, 2012; revised May 12, 2012; accepted July 03, 2012. Date of publication July 11, 2012; date of current version July 31, 2012. This work has been carried out at the "Institut d'Electronique et de Télécommunications de Rennes", IETR, Rennes, France. The project was financed by Thales Alenia Space, France.

S. A. Muhammad, A. Rolland, S. H. Dahlan, and R. Sauleau are with IETR, UMR CNRS 6164, University of Rennes 1, 35042 Rennes, France (e-mail: mshoaibanwar@yahoo.com; anthony.rolland@univ-rennes1.fr; samsulh@uthm.edu.my; ronan.sauleau@univ-rennes1.fr).

H. Legay is with Thales Alenia Space, France, 31037 Toulouse Cedex 1, France (e-mail: herve.legay@thalesaleniaspace.com).

Color versions of one or more of the figures in this letter are available online at http://ieeexplore.ieee.org.

Digital Object Identifier 10.1109/LAWP.2012.2208259

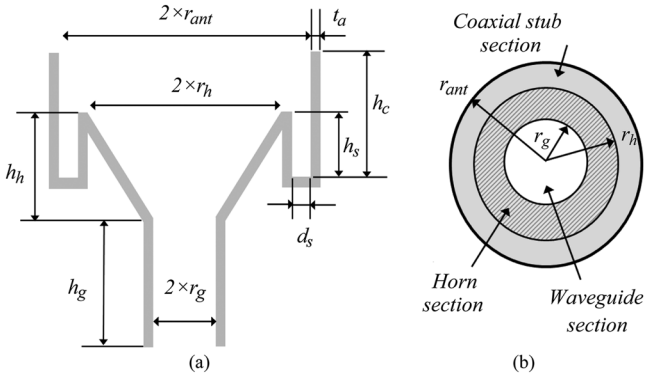

Fig. 1. (a) Cross-section view and (b) top view of the Scrimp horn antenna.

TABLE I
OPTIMIZATION GOALS FOR THE SCRIMP HORN

Parameter	Goal
Frequency bandwidth	3.7 – 4.2 GHz (12.6%)
Aperture efficiency	≥ 70%
Reflection coefficient	≤ - 20 dB
Side lobe level	≤ - 25 dB

The main optimization goals, provided by Thales Alenia Space, France, are defined in Table I. Here, the aperture efficiency is defined as

$$A_{\mathrm{e}} = \frac{D(f) \bullet \lambda_0^2}{4\pi S} \tag{1}$$

where $D(f)$ is the antenna directivity, λ_0 is the wavelength in free space, and S is the aperture area ($S = \pi\, r_{\mathrm{ant}}^2$).

The global cost function $\mathrm{CF_g}$ is defined as the sum of the contribution of each goal defined in Table I

$$\mathrm{CF_g} = \mathrm{CF_{Ae}} + \mathrm{CF_{S11}} + \mathrm{CF_{SLL}} \tag{2}$$

where $\mathrm{CF_{Ae}}$, $\mathrm{CF_{S11}}$, and $\mathrm{CF_{SLL}}$ are the individual cost functions for the aperture efficiency, the reflection coefficient, and the sidelobe level, respectively

$$\mathrm{CF_{Ae}} = \sum_{i=1}^{N_{\mathrm{f}}} \frac{\max^2\left(\eta_{\mathrm{s-Thr}} - \eta_{s-Ant}(f_i, \theta_0)\right)}{N_{\mathrm{f}}} \tag{3}$$

$$\mathrm{CF_{S11}} = \sum_{i=1}^{N_{\mathrm{f}}} \frac{\max\left(S_{11-\mathrm{Ant}}(f_i) - S_{11-\mathrm{Thr}}\right)}{N_{\mathrm{f}}} \tag{4}$$

$$\mathrm{CF_{SLL}} = \sum_{i=1}^{N_{\mathrm{f}}} \frac{\sum_{j=1}^{N_\theta} \frac{\max(F_1(f_i,\theta_j)) + \max(F_2(f_i,\theta_j))}{N_\theta}}{N_{\mathrm{f}}} \tag{5}$$

where

$$F_1(f_i, \theta_j) = \mathrm{SLL_{Ant}}^{E}(f_i, \theta_j) - \mathrm{SLL_{Thr}} \tag{6}$$

$$F_2(f_i, \theta_j) = \mathrm{SLL_{Ant}}^{H}(f_i, \theta_j) - \mathrm{SLL_{Thr}}. \tag{7}$$

Here, N_{f} is the number of frequency points over which the optimization is carried out ($N_{\mathrm{f}} = 5$ here), $\eta_{\mathrm{s-Thr}}$ and $\eta_{\mathrm{s-Ant}}$ are the threshold values and actual antenna aperture efficiencies respectively at each frequency point f_i and for $\theta_0 = 0°$ (broadside), $S_{11-\mathrm{Thr}}$ and $S_{11-\mathrm{Ant}}$ are the threshold values and actual antenna reflection coefficient respectively at each frequency point f_i. Similarly, $\mathrm{SLL_{Thr}}$, $\mathrm{SLL^{E}_{Ant}}$, and $\mathrm{SLL^{H}_{Ant}}$ are the sidelobe values at threshold and E- and H-planes at f_i and for the elevation angle θ_j [$N_\theta = 61$ (3° step), by considering solely half a pattern by plane of interest due to the axis symmetry]. The threshold values used here are the ones indicated in Table I.

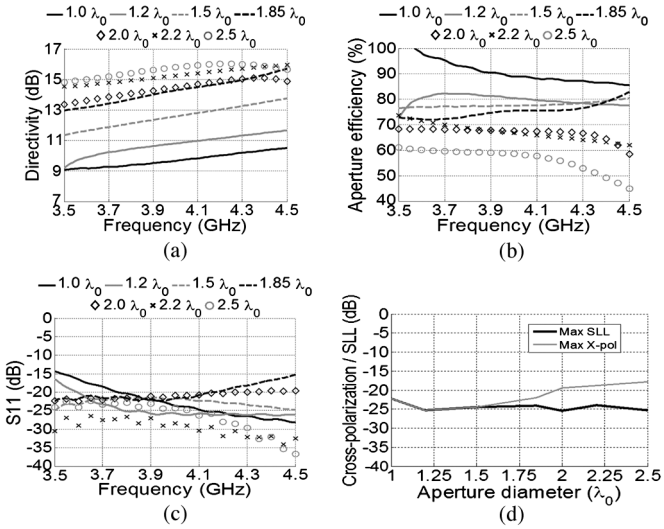

Fig. 2. BoR-FDTD optimization results for the different aperture diameters. (a) Directivity. (b) Aperture efficiency. (c) Reflection coefficient. (d) Maximum sidelobe level (SLL) and cross-polarization levels (X-pol).

TABLE II
OPTIMIZED DIMENSIONS OBTAINED WITH THE BOR-FDTD TOOL

	Aperture diameter $2\times r_{ant}$ (in λ_0)						
Dimensions (mm)	1.0	1.2	1.5	1.85	2.0	2.2	2.5
$2\times r_{ant}$	76	92	115	142	154	169	192
r_h	34.5	40.8	46.4	52.8	55.3	73.4	82.8
h_h	23.9	36.2	44.4	35.2	36.8	73.5	70.1
h_s	21.7	18.6	16.5	15.3	18.8	21.5	18.3
h_c	22.4	20.0	40.3	56.2	47.3	40.3	40.5
d_s	3.9	5.3	11.3	18.3	21.6	11.2	13.3

If each individual goal is met, the global cost function is equal to zero. If this is not the case, the final result is based on the best performance in terms of aperture efficiency.

The optimization procedure has been carried out for seven antenna aperture sizes $2\times r_{\mathrm{ant}}$ ranging from λ_0 to $2.5\lambda_0$ in C-band around a central frequency of 3.95 GHz ($\lambda_0 = 75.95$ mm). In all cases, the waveguide dimensions are fixed ($r_{\mathrm{g}} = 29.225$ mm, $h_{\mathrm{g}} = 25$ mm), and the maximum allowed height for the antenna is fixed at λ_0 (without the excitation waveguide part h_{g}). The dimensions of the smooth-wall conical section of the horn and its coaxial stub part are automatically varied (Fig. 1) during optimization. The antenna wall thickness (t_{a}) is assumed to be zero; several independent runs were launched in each case, and the best solution was selected.

C. Optimization Results

The final dimensions obtained after optimization are summarized in Table II for the seven aperture sizes. The antenna performance curves for all cases are provided in Fig. 2. The variation of directivity over the simulated frequency band is presented in Fig. 2(a). A linear increase in directivity can be observed over the optimized frequency band (3.7–4.2 GHz).

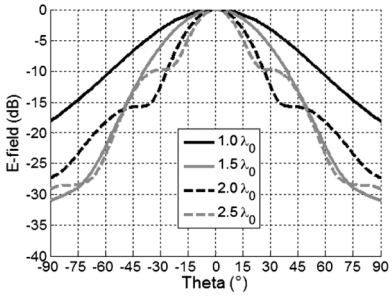

Fig. 3. Radiation patterns in E-plane for various aperture sizes at 4.2 GHz.

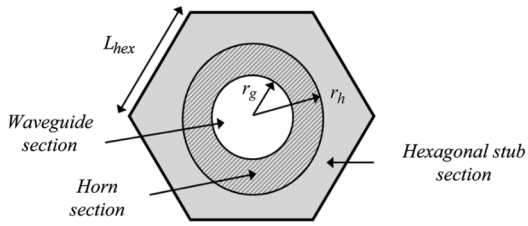

Fig. 4. Hexagonal scrimp horn antenna.

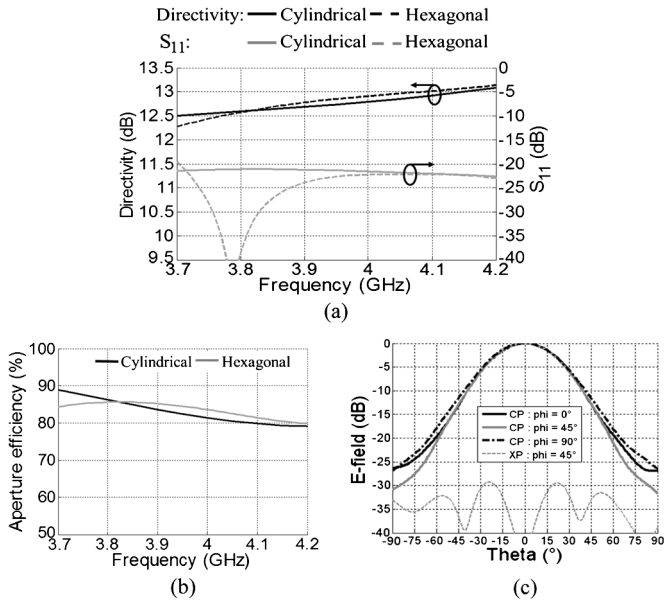

Fig. 5. HFSS simulation results for the optimized Scrimp horn with cylindrical and hexagonal apertures. (a) Directivity and reflection coefficient. (b) Aperture efficiency. (c) Radiation patterns at 3.95 GHz.

Fig. 2(b) shows that, for aperture diameters ranging between λ_0 and $1.85\lambda_0$, high aperture efficiencies ($>$70%) are maintained over the 3.7–4.2-GHz frequency band. The value at lower frequencies is larger than 100% for the λ_0 case because "S" in (1) is the geometrical surface area and not the unwrapped one. For larger apertures, the 70% limit could not be satisfied with a maximum antenna height of λ_0. Reflection coefficients lower than -20 dB are satisfied for all cases [Fig. 2(c)]. A maximum sidelobe level of -24 dB is maintained over the entire bandwidth for aperture diameter larger than λ_0 [Fig. 2(d)], while the maximum cross-polarization level is degraded as the aperture size is increased beyond $1.85\lambda_0$. This maximum is calculated taking into account four observation planes ($\varphi = 0°$, 45°, 90°, or 135°). The E-plane patterns for the varying aperture sizes are shown in Fig. 3 as an example. The highest frequency (4.2 GHz) is selected because this is where we obtain the worst-case patterns. It can be observed that with the increase in aperture size, the pattern quality is slightly deteriorated by shouldering effects (Fig. 3) and axial dissymmetry (not shown here).

III. Hexagonal Scrimp Horn Antenna

A. Design

The $1.5\lambda_0$ Scrimp horn configuration has been selected for further study due to its excellent performance and very compact size suitable for a multibeam focal array system. The geometry of the horn was modified in such a way that the coaxial part [Fig. 1(b)] was replaced by a hexagonal one with the same area in order to obtain the same aperture efficiency as for a cylindrical aperture. This hexagonal shape allows a better integration into an array configuration (Fig. 4). The specifications to be met are the same as in Table I.

B. Simulation Results

This antenna model has been simulated with HFSS. Its dimensions are the same as in Table II, except for the hexagonal part ($L_{\rm hex} = 63.5$ mm) and the thickness $t_{\rm a}$ that has been fixed to 3 mm in order to obtain a realistic and mechanically rigid prototype. The total height of the horn is only 96.3 mm ($1.25\lambda_0$), and it operates in linear polarization.

The numerical results are shown in Fig. 5. The characteristics of the Scrimp horn with cylindrical aperture (Fig. 2) are also provided for comparison purposes. The directivity curves almost superimpose [Fig. 5(a)] for the cylindrical and hexagonal cases. The impedance-matching levels remain below -20 dB in both cases. The dip in the S_{11} curve of the hexagonal case is due to the resonance of the feeding network (the details of which are out of the scope of this letter). The aperture efficiency curves [Fig. 5(b)] are also in excellent agreement with levels higher than 80% over the total desired bandwidth.

The radiation patterns [Fig. 5(c)] computed at the central frequency (3.95 GHz) are of excellent quality with cross-polarization levels lower than -28 dB and sidelobes lower than -25 dB. The symmetry in the patterns is maintained over the entire frequency bandwidth with maximum sidelobe and cross-polarization levels reaching -24 and -27 dB, respectively.

C. Experimental Results

The antenna is in aluminum and was fabricated in separate parts. The horn section iss machined with the waveguide and assembled to the hexagonal cavity. The final assembled antenna with its feed is shown in Fig. 6. The height of the antenna without the feeding part is $1.26\lambda_0$. The antenna aperture and feed are fabricated inside a cylindrical block due to ease of fabrication. In an array configuration, it can be imagined that several hexagonal feeds are machined side by side in one large metallic block.

The antenna was measured in the centimeter-wave far-field anechoic chamber of IETR, Rennes, France, in linear polarization using a reference 12-dB horn. The measured directivity [Fig. 7(a)] varies between 12.2 and 13.2 dB. The realized gain

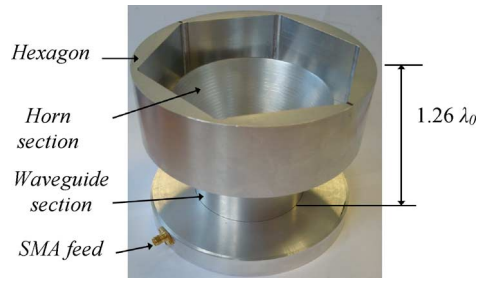

Fig. 6. Prototype in *C*-band.

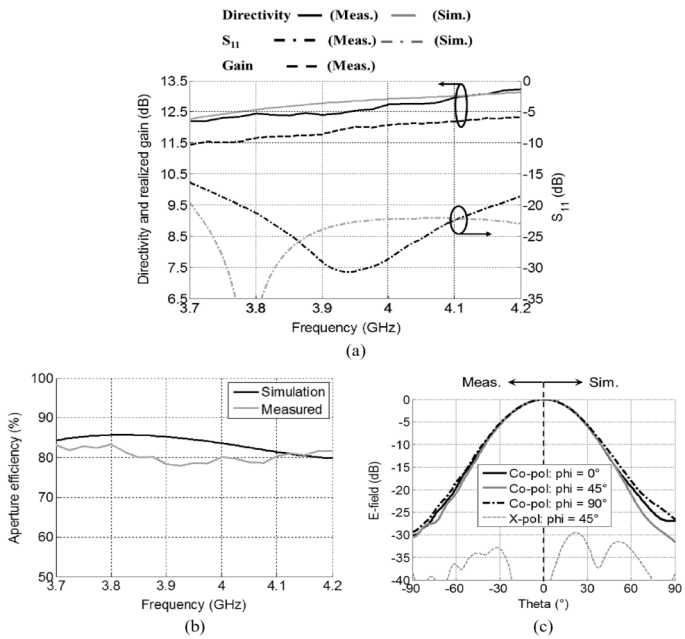

Fig. 7. Simulation and experimental results for the prototype. (a) Directivity, realized gain, and reflection coefficient. (b) Aperture efficiency. (c) Radiation patterns at 3.95 GHz.

curve is about 0.8 dB below the directivity curve. This difference is due to the losses in the printed feeding network. The measured reflection coefficient remains below -17 dB over the entire bandwidth

The measured aperture efficiency is in very good agreement with the simulations [Fig. 7(b)]. The radiation patterns measured at 3.95 GHz [Fig. 7(c)] are axially symmetric and exhibit very low sidelobes and cross-polarization levels.

IV. Conclusion

An optimization tool based on the BoR-FDTD solver coupled with a genetic algorithm is applied to Scrimp horns first presented in [11] and [12]. The proposed tool is applied to optimize several antennas with different aperture sizes while minimizing the antenna size and satisfying the given performance requirements of Table I.

It can be concluded that these antennas produce excellent performance for apertures lower than $2\lambda_0$ with antenna height between $0.32\lambda_0$ and $0.86\lambda_0$ (without the feeding waveguide part fixed at $0.33\lambda_0$).

Next, a hexagonal Scrimp horn operating in C-band has been designed with an aperture of $1.5\lambda_0$. Both simulation and experimental results showed excellent performance with aperture efficiency levels greater than 80% over a 12.6% frequency bandwidth and axially symmetric radiation patterns with low sidelobes and cross-polarization levels for a total antenna height of only $1.26\lambda_0$. The antenna satisfied all the performance parameters defined in Table I. The performance of the proposed antenna is compared to other solutions in the literature in Table III. It can be observed that the Scrimp horn presents an attractive alternative to other compact antenna solutions with excellent performance.

TABLE III
Comparison of Proposed Scrimp Horn With Solutions in Literature

Antenna type	Aperture (λ_0)	Height (λ_0)	Operational bandwidth (%)	Side lobe levels (dB)
Corrugated horns [4]	≤ 15	≥ 5	≥ 10	Very low
Potter horns [6]	≥ 2	≥ 2	≥ 10	Very low
Stacked FP [10]	1.85	~ 1	10	$\leq$ -20
SBA [7]	≤ 2	≤ 1	≤ 10	$\leq$ -15
Scrimp horn (this work)	1.5	0.86	12.6	$\leq$ - 25

The perspective of this work is the evaluation of this design for (single and dual) circular polarization operation and for a particular focal array application.

References

[1] A. W. Love, *Reflector Antennas*. New York: IEEE Press, 1978.
[2] C. L. Kory, K. M. Lambert, R. J. Acosta, and J. A. Nessel, "Prototype antenna elements for the next generation TDRS enhanced multiple access array," *IEEE Antennas Propag. Mag.*, vol. 50, no. 4, pp. 72–83, Aug. 2008.
[3] C. Granet, T. S. Bird, and G. L. James, "Compact multimode horn with low sidelobes for global Earth coverage," *IEEE Trans. Antennas Propag.*, vol. 48, no. 7, pp. 1125–1133, Jul. 2011.
[4] C. Granet, "Design of a compact C-band receive only horn for Earth station antenna G/T_A performance," *IEEE Antennas Wireless Propag. Lett.*, vol. 2, pp. 294–297, 2003.
[5] P. D. Potter, "A new horn antenna with suppressed side lobes and equal beamwidths," *Microw. J.*, vol. VI, no. 6, pp. 77–81, Jun. 1963.
[6] H. Deguchi, E. Tsuji, and H. Shigesawa, "Compact low cross-polarization horn antennas with serpentine shaped taper," *IEEE Trans. Antennas Propag.*, vol. 52, no. 10, pp. 2510–2516, Oct. 2004.
[7] D. Gray, H. Tsuji, and Y. Fujino, "Low profile feed for wide scan flat plate reflector antenna," *IEICE Tech. Rep.*, vol. 108, AP2008-198, no. 429, pp. 55–60, Feb. 2009.
[8] P. Ingvarson, U. Jostell, and P. Svedjenas, "Pach excited cup elements for satellite based mobile communication antennas," in *Proc. IEEE Int. Conf. Phased Array Syst. Technol.*, Dana Point, CA, May 2000, pp. 215–218.
[9] C. A. Balanis, *Antenna Theory: Analysis and Design*. New York: Wiley, 2005, ch. 12, p. 600.
[10] S. A. Muhammad, R. Sauleau, and H. Legay, "Small-size shielded metallic stacked Fabry–Perot cavity antennas with large bandwidth for space applications," *IEEE Trans. Antennas Propag.*, vol. 60, no. 2, pp. 792–802, Feb. 2012.
[11] H. Wolf and E. Sommer, "An advanced compact radiator element for multi-feed antennas," in *Proc. 18th Eur. Microw. Conf.*, Stockholm, Sweden, 1988, pp. 506–511.
[12] E. Dudok, N. Nathrath, E. Sommer, H. Wolf, and G. Crone, "Development of a multi-shaped beam antenna in C-band," in *Proc. 19th Eur. Microw. Conf.*, London, U.K., Sep. 1989, pp. 1110–1117.
[13] A. Rolland, M. Ettorre, M. Drissi, L. Le Coq, and R. Sauleau, "Optimization of reduced-size smooth-walled conical horns using BoR-FDTD and genetic algorithm," *IEEE Trans. Antennas Propag.*, vol. 58, no. 9, pp. 3094–3100, Sep. 2010.